Temperature Rise Calculation and Velocity Planning of Permanent Magnet Linear Synchronous Motor under Trapezoidal Speed

Xuzhen Huang, *Member, IEEE*, Zheng Wang, Yiwei Zhang, and Qiang Tan

***Abstract*—For permanent magnet linear synchronous motor (PMLSM) working at trapezoidal speed for long time, high thrust brings high temperature rise, while low thrust limits dynamic performance. Thus, it is crucial to find a balance between temperature rise and dynamic performance. In this paper, a velocity planning model of the PMLSM at trapezoidal speed based on electromagnetic-fluid-thermal (EFT) field is proposed to obtain the optimal dynamic performance under temperature limitation. In this model, the winding loss is calculated considering the acceleration and deceleration time. The loss model is indirectly verified by the temperature rise experiment of an annular winding sample. The actual working conditions of the PMLSM are simulated by dynamic grid technology to research the influence of acceleration and deceleration on fluid flow in the air gap, and the variation rule of the thermal boundary condition is analyzed. Combined with the above conditions, the temperature rise of a coreless PMLSM (CPMLSM) under the rated working condition is calculated and analyzed in detail. Through this method and several iterations, the optimal dynamic performance under the temperature limitation is achieved. The result is verified by a comparison between simulation and prototype tests, which can help improve the dynamic performance.**

***Index Terms*—Permanent magnet linear synchronous motor, temperature rise, velocity planning, electromagnetic-fluid-thermal field, dynamic performance.**

I. Introduction

In the application of processing, manufacturing and logistics transportation, permanent magnet linear synchronous motor (PMLSM) often works at the trapezoidal speed curve as shown in Fig. 1 and makes periodic reciprocating motion [1]-[5]. In order to finish the work within the specified time (such as material transportation, etc.), the maximum speed and acceleration limits are usually given. The acceleration, deceleration and uniform motion time of the mover are planned by motion controller. In this case, for the sake of the thermal safety of the PMLSM, leaving a large margin is usually adopted to limit the motor temperature rise. In this way, the excessive margin is often selected, resulting in the mismatch between the work beat and production efficiency of the equipment equipped.

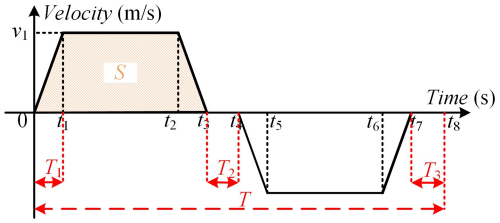

Fig. 1. Trapezoidal speed of PMLSM.

When the operating state of PMLSM switches between acceleration, deceleration and uniform motion, the loss during the acceleration or deceleration is much higher than that during uniform motion, and the temperature rises rapidly [6]. The selection of the acceleration and maximum speed is not only closely related to the thrust performance but also has a complex nonlinear relationship with the electromagnetic loss and temperature rise. Furthermore, it determines the dynamic performance of the PMLSM. Therefore, in practical application, it is significant to consider both the electromagnetic thrust and the temperature rise limit.

Many scholars have carried out theoretical research on the temperature rise calculation and velocity planning of PMLSM. In terms of temperature rise calculation, there are two main methods: thermal circuit and numerical method [7]-[10]. The thermal circuit method is computationally efficient, but the density of the nodes determines the calculation accuracy [7], [9]. The numerical method is suitable to model and analyze the temperature distribution in detail but requires a complicated modelling process and longer calculation time [11]. The advantages of thermal circuit and numerical method are integrated in [12]. The combined model of thermal circuit and temperature field of a tubular PMLSM is established to calculate the transient temperature rise. The fluid field model of PMLSM is simplified and separated from the coupling calculation, which greatly reduces the calculation time and improves the practicability [13]. To explore the relationship between the electromagnetism and thermal behavior of PMLSM, a two-dimensional (2D) finite element model (FEM) of the electromagnetism-thermal coupling based on a double

Manuscript received June 22, 2022; revised August 03, 2022; accepted August 15, 2022. date of publication September 25, 2022; date of current version September 18, 2022.

This work was supported in part by the National Natural Science Foundation of China under Grant 52022040, in part by the Postgraduate Research & Practice Innovation Program of NUAA. (*Corresponding Author: Xuzhen Huang)*.

Xuzhen Huang, Zheng Wang, Yiwei Zhang, Qiang Tan are with the Department of Electrical Engineering, Nanjing University of Aeronautics and Astronautics, Nanjing 210016, China (e-mail: huangxuzhen@nuaa.edu.cn; wongzheng@nuaa.edu.cn; zywnuaa@126.com; tanqiang0213@nuaa.edu.cn)

Digital Object Identifier 10.30941/CESTEMS.2022.00032

closed-loop algorithm is proposed, which comprehensively considers all materials and doubles the motor thrust with small water flow rate [14]. In addition, the fluid model of the PMLSM air gap is established by using the FEM, and the law of the airflow on each surface is obtained, which provides a basis for thermal analysis [15].

In the aspect of velocity planning, most researches are carried out from drive control. For example, the general algorithm of S-curve motion trajectory design is put forward in [16], which has high efficiency and application ability. The motion curve of PMLSM is designed to a sinusoidal curve, which reduces the machine tool vibration at the same execution time [17]. A double loop control structure is developed to maximize the convergence speed and achieve high steady-state accuracy [18].

There exist some questions that the above calculations on the temperature rise of PMLSM have not considered the differences of the loss, heat exchange, temperature when the motor works in the different speed curve. The existing motion planning is usually out of consideration of thermal factors as well, resulting in the failure of the dynamic performance of PMLSM to reach the optimal state.

This paper focuses on a velocity planning model of PMLSM at trapezoidal speed based on electromagnetic-fluid-thermal (EFT) model. The EFT model of a coreless PMLSM (CPMLSM) is established, which considers the acceleration and deceleration state. The velocity curve is planned and the optimal dynamic performance under the temperature limitation is obtained. This paper mainly focuses on the change of the temperature rise and dynamic performance with the acceleration and deceleration state of the motor. The main contents include: In Section II, the structure and thrust characteristics of the CPMLSM are introduced. In Section III, the loss and fluid models considering the value and time of the acceleration and deceleration are established and verified. In Section IV, the velocity planning model of PMLSM at trapezoidal speed based on EFT field is proposed. The temperature distribution is calculated and the dynamic performance is optimized. The temperature rise and dynamic performance of a PMLSM prototype are verified in Section V. Finally, the conclusions are drawn in Section VI.

II. Structure and Thrust of the CPMLSM

The structure of the CPMLSM is shown in Fig. 2. The primary is used as the mover, which is composed of windings and epoxy resin. The windings are mainly filled with epoxy resin to fix brackets and insulation. The secondary is used as the stator, which is composed of permanent magnets (PMs) and back yokes. The PMs adopt surface-mounted parallel magnetized magnetic poles. x, y and z of the triangular coordinate system represent the transverse, radial and axial directions of PMLSM. The main parameters of the prototype are shown in Table I.

Fig. 3 shows the average thrust under different sinusoidal load currents and the maximum thrust variation with speed under limited power supply. The control method is $i_d = 0$. The output thrust changes linearly with load current. It can well

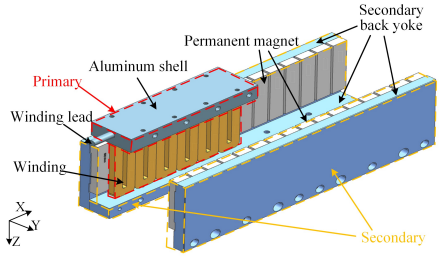

Fig. 2. The structure of the CPMLSM.

TABLE I
CPMLSM PARAMETERS

Parameters	Value	Unit
Primary length	120	mm
Coil height	5.1	mm
Coil width	20	mm
Turns of coil	120	--
PM height	7	mm
PM width	13	mm
Pole pitch	15	mm
Airgap length	1.05	mm
Rated speed	1.5	m/s
Rated current	2.53	A
Rated thrust	80	N
Stroke	240	mm

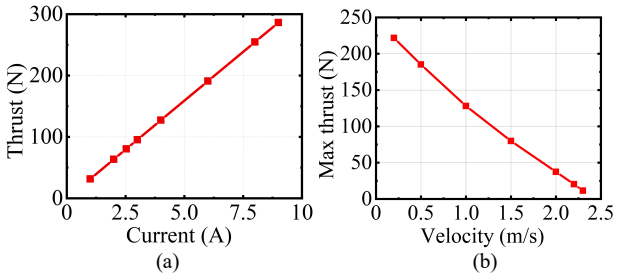

Fig. 3. Thrust changes with (a) current, (b) velocity.

adapt to the application scenario of large-scale change of load thrust. At the same time, when the mover speed is low, the peak value of the thrust is large. Considering the thermal limit, it is possible for the CPMLSM to operate under short-term high overload conditions.

III. Thermal Model of the CPMLSM

A. Loss Model

During the operation of the PMLSM, it is inevitable to produce copper loss, core loss, eddy current loss in PMs, mechanical loss [19]-[21]. Since the CPMLSM doesn't have an iron core structure, there is no core loss in the primary. The eddy current loss in PMs can be neglected due to the low-rated supply frequency. The mechanical loss can be calculated by empirical formula. Thus, copper loss is only considered emphatically.

When the CPMLSM works at trapezoidal speed as shown in Fig. 1, the time the mover spent in making a reciprocating motion is considered as a period, defined as T. The acceleration and deceleration time are the same, defined as T_1. The waiting intervals between each unidirectional movement are T_2 and T_3 respectively, in which the motor loads objects, etc. Then, the proportion of acceleration and deceleration time D during a period is

$$D = 4T_1 / T, 0 < D \le 1 \quad (1)$$

The proportion of the waiting intervals is

$$\mu = (T_2 + T_3) / T, 0 \le \mu < 1 \quad (2)$$

The stroke of the mover is S, which is a constant. Under low-frequency speed response conditions, copper loss is determined by the current value and resistance. When the PMLSM operates in a periodic state, the current changes periodically and the copper loss changes accordingly. The motion equation and thrust formula of the CPMLSM in a round trip are as follows

$$ma = F_{em} - B_v v \pm F_f \quad (3)$$

$$F_{em} = K_f i_q \quad (4)$$

where m, a, v is the mass, acceleration and velocity of the mover, respectively. F_{em}, B_v, K_f and i_q is the electromagnetic thrust, viscous friction coefficient, thrust coefficient and the q-axial current, respectively. F_f is the friction resistance.

The effective phase current is obtained according to the conversion relationship between the three-phase and the two-phase rotating coordinate system. The average effective current I_0 can be calculated by the effective phase current.

$$3\sum_{i=1}^{3} I_i^2 R t_i = 3I_0^2 R t_0 \quad (5)$$

where I_i (i = 1,2,3,4,5) are the effective phase currents in acceleration, deceleration, uniform speed and two waiting intervals, respectively. t_i (i = 1,2,3,4,5) are the times when the motor starts acceleration, deceleration, uniform speed, and two waiting intervals, respectively. R is the coil resistance. t_0 is the total time required for the motor making a round trip. The copper loss of the motor in a round trip can be calculated through the average effective current.

$$P_{Cu} = 3I_0^2 R = \frac{3}{2} R[(I_1^2 + I_2^2)D + 2I_3^2(1 - D - \mu)] \quad (6)$$

Because the current is determined by the acceleration concluded from (1), (2), the effective phase currents I_1 and I_2 during the acceleration and deceleration are much greater than the current I_3 at uniform speed. The waiting intervals are determined by the specific application of the PMLSM. Since the goal of this paper is to study the influence of the acceleration and deceleration on thermal condition, an assumption is made that the proportion of the waiting intervals is zero (μ=0). Thus, equation (6) can be expressed as

$$P_{Cu} = 3I_0^2 R = \frac{3}{2} R[(I_1^2 + I_2^2)D + 2I_3^2(1 - D)] \quad (7)$$

According to the acceleration a in the velocity planning, the copper loss under the different proportion of acceleration and deceleration time D can be calculated. Fig. 4 shows the copper loss under different acceleration a and the acceleration and deceleration time D. When the proportion of acceleration and deceleration time D or acceleration a increases, the copper loss increases concomitantly.

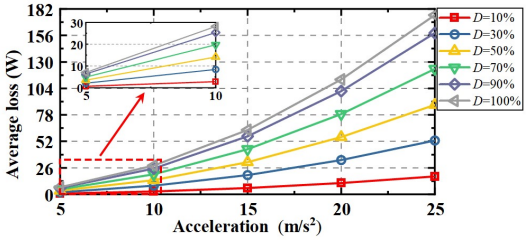

Fig. 4. Copper loss under different acceleration a, and proportion of acceleration and deceleration time D.

B. *Verification for the Loss Model*

The winding loss model under different acceleration and proportion of acceleration and deceleration time is indirectly verified by testing the temperature rise of a single winding sample. The annular winding sample used in the flat PMLSM and the test platform are shown in Fig. 5. The annular winding sample adopts the self-adhesive wires with a diameter of 0.5 mm, the insulation level of which is F. The temperature rises on the outer surface and inside the annular winding sample are obtained by the thermistor and thermal imager.

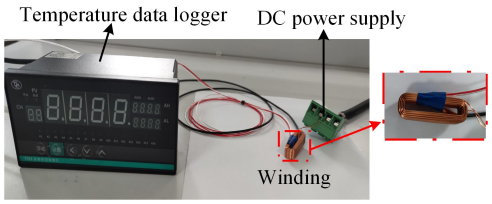

Fig. 5. Test platform and annular winding sample.

When calculating the annular winding sample temperature, the equivalent layered conductor model is adopted [22]-[23]. Table II shows the thermal parameters of the conductor and the insulation layers. The surface of the annular winding is under natural convection.

TABLE II
MATERIAL THERMAL PARAMETERS

Part	Thermal conductivity W/(m·K)	Density kg/m³	Specific heat capacity J/(kg·K)
Conductor layer	400	8900	390
Insulation layer	0.35	1230	1560

The annular winding is powered on with current density of 10 A/mm^2. The period T is 8 s. The percentage of power-on time, which refers to the proportion of acceleration and deceleration time D, is 25%, 50% and 75%, respectively. The families of the calculated and tested temperature rise curves on the outer surface of the annular winding sample are shown in Fig. 6. They are satisfied well with each other and the maximum temperature difference is no more than 4 ℃. When the annular winding sample reaches the heat balance, the tested values of the outer surface temperature are 47, 71 and 97.90 ℃, while the corresponding calculated values are 47.93, 73.60 and 101.04 ℃, respectively.

Meanwhile, the working environment of the PMLSM is diverse, and short-time high overload is one of the most common working conditions. In order to obtain the calculation accuracy of the loss model under the condition of short-time and high overload, the annular winding sample is powered on with current density of 30 A/mm^2. The period T is also 8 s. The percentage of power-on time is selected as 25%, 50% and 75% as well. Considering the insulation limit, the corresponding power-on times are 2.4, 1.1 and 0.7 minutes, respectively. The

tested and calculated results are shown in Fig. 7. The tested values of the maximum winding temperature are 137.30, 130.20 and 134 ℃, respectively. The corresponding calculated values are 135.76, 135.59 and 135.11 ℃. The tested values of the outer surface of the annular winding sample are 109.10, 90.40 and 89.10 ℃, respectively. The corresponding calculated values are 109.29, 92.43 and 91.21 ℃. The errors between the tested and the calculated values are basically controlled within 5%. Compared Fig. 7 (a) and (b), under short-time high overload working conditions, the winding temperature gradient is larger and there is more severe heating inside the windings.

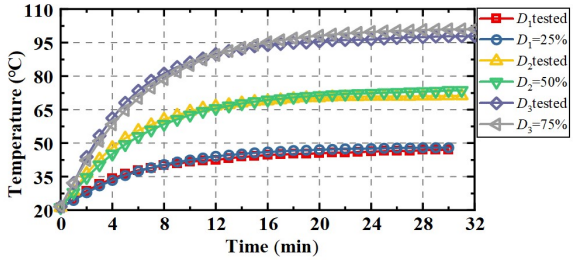

Fig. 6. Tested and calculated temperature rise with the current density of 10 A/mm^2.

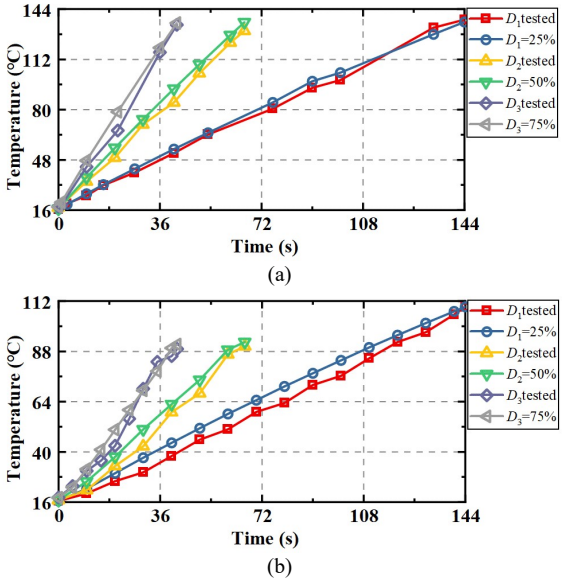

Fig. 7. Tested and calculated temperature rise with the current density of 30 A/mm^2. (a) Maximum temperature. (b) Outer surface temperature.

The above results indirectly prove the validity of the loss model.

C. Heat Transfer Coefficient

Operating under complex working conditions, the convective heat transfer coefficient of the PMLSM is a complicated function depending on a variety of physical factors, such as fluid velocity, density, dynamic viscosity, thermal conductivity and specific thermal pressure [24]-[25]. The outer surface of the CPMLSM stator is in the natural cooling state. The heat transfer coefficient can be selected or calculated according to the experience and related theory.

The air gap surface is in forced convection state. Since the CPMLSM is in the state of frequent reciprocating acceleration and deceleration and the mover is located between the stator interlayer, the airflow in the air gap is complex. The dynamic grid method is used to simulate the actual working conditions of the PMLSM and research the airflow characteristics in the air gap. On this basis, the influence of different working conditions on the convective heat transfer coefficient is studied, improving the accuracy of temperature rise prediction.

Referring to [13], [15], ignoring the intervals between the PMs and influence of the temperature on the airflow on the outer surface, a 2D model of the CPMLSM fluid field model based on the dynamic grid method is established. The specific boundary conditions are as follows:

1) Ignoring the influence of buoyancy and gravity, the air is an incompressible ideal gas.

2) According to the Reynolds number, the laminar flow model is adopted.

3) A standard atmospheric pressure is taken as the initial value, and the inlet and outlet are set as pressure boundary conditions.

4) The contact surfaces between the motor and the air are set as no-slip conditions, and the mover is given the actual motion form by profile.

The velocity distribution of the airflow in the CPMLSM air gap under different operating states is shown in Fig. 8. The airflow is unstable and some vortexes exist when the mover operates in an acceleration and deceleration state. Whereas, the velocity of the airflow is generally distributed in layers. Due to the existence of viscous force, the air velocity near the stator side is approximately zero and that near the mover side is close to the velocity of the mover.

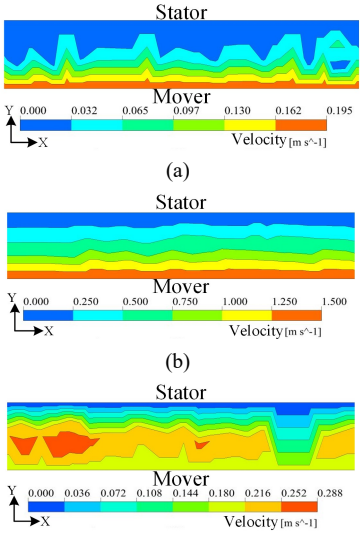

Fig. 8. Velocity distribution of air flow in the coreless PMLSM air gap. (a) Acceleration, v = 0.195 m/s, a = 15 m/s^2. (b) Uniform speed, v =1.5 m/s, a = 0 m/s^2. (c) Deceleration, v = 0.195 m/s, a = - 15 m/s^2.

The value of the air velocity in the air gap and the air velocity in x-direction under different working conditions are calculated respectively for further research, as shown in Fig. 9. The air velocity is basically the same in the x-direction. There exists only a slight difference in the initial acceleration stage of the mover, which indicates that the airflow in the air gap mainly flows in the x-direction. In addition, at the beginning of the movement, the air flows in the opposite direction of mover motion, but the duration is too short. When the mover reaches

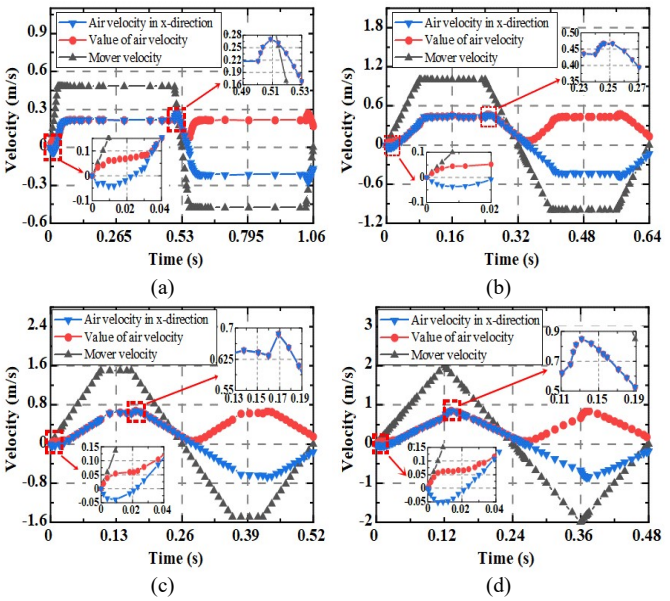

Fig. 9. Air velocity in air gap under different working conditions. (a) D=11.32%, v_{max}=0.48m/s. (b) D=50%, v_{max}=1m/s. (c) D = 76.9%, v_{max}=1.5m/s. (d) D=100%, v_{max}=2m/s.

the uniform speed, the airflow also enters the same state after a lag. At the time mover begins to decelerate, the air velocity has an upward tendency, which lasts shorter. In general, compared with the mover velocity variation, the airflow variation lags slightly.

The existing references about fluid field calculation of the PMLSM mostly assume that the motor is stationary, and the inlet of fluid field model is set as velocity boundary, given an equivalent wind speed. The influence of acceleration and deceleration on the airflow is ignored. However, as shown in Fig. 9, the air velocity in the air gap is closely related to the acceleration and deceleration state. It directly affects the convective heat transfer coefficient.

According to the above analysis, the fluid velocity in one cycle is averaged to simplify the calculation. The heat transfer coefficient of the air gap surface is calculated as [26]

$$h = Nu\lambda/l \tag{8}$$

$$Nu = 0.16Re^{0.699} \tag{9}$$

$$Re = ul/v \tag{10}$$

where h is the convective heat transfer coefficient and Nu is the Nusselt number. λ is the thermal conductivity; l is the length of the air gap; Re is the Reynolds number. u is the mover velocity, and v is the kinematic viscosity of air.

Fig. 10 shows the air velocity and convective heat transfer coefficients. The average value of the air velocity without considering the acceleration and deceleration is greater than that considering the acceleration and deceleration state. The difference between them gradually rises with the proportion of acceleration and deceleration time increasing, from 0.02 m/s to 0.33 m/s, resulting in the maximum error of 19 W/(m^2·K) in heat transfer coefficient. In addition, although the max velocity of the mover increases by 0.5 m/s at D = 1 compared with that in D = 0.8, it has little impact on the average value of air velocity, only increasing by 0.033 m/s. The increase of the heat transfer coefficient is limited consequently. Rising the acceleration and deceleration time to increase the mover speed has a limited positive impact on the motor heat dissipation. Combining other methods to enhance motor heat dissipation capacity is necessary.

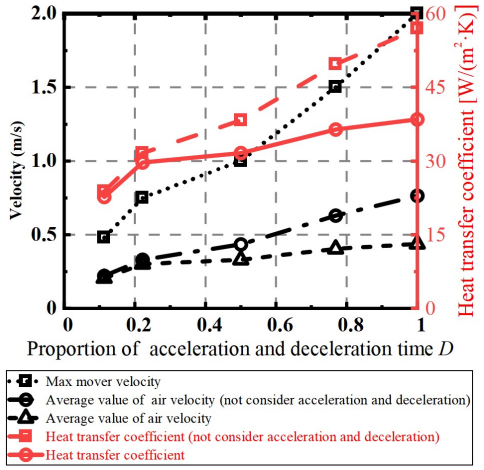

Fig. 10. Air velocity and heat transfer coefficients.

IV. Temperature Rise Calculation and Velocity Planning of PMLSM Based on Multi-physical Field

A. Temperature Calculation Model and Velocity Planning

For the PMLSM with a certain stroke and operating at trapezoidal speed, its speed trajectory is fixed when the proportion of acceleration and deceleration time D and the acceleration a are determined. Therefore, the temperature rise calculation and velocity planning should be carried out at the same time. In industrial material transmission, the dynamic performance of PMLSM, determined after the velocity planning, is often evaluated by the number of round trips per second, which is defined as n.

$$n = 0.25\sqrt{\frac{aD(2-D)}{S}} \tag{11}$$

n is closely related to the proportion of acceleration and deceleration time D and acceleration a, and improved with their increase. The model of temperature calculation and velocity planning is given in this section to obtain the optimal dynamic performance under the insulation limit. The flowchart is shown in Fig. 11.

The acceleration a and the proportion of acceleration and deceleration time D are firstly given during PMLSM velocity planning. Then, the average thrust, as well as dynamic performance, is calculated. Much more, the acceleration a and the proportion of acceleration and deceleration time D are the input conditions of the electromagnetic field and fluid field, where the electromagnetic loss as the heat source and the heat transfer coefficient as the boundary condition are gained. Combined with the two factors, the PMLSM thermal field is simulated and analyzed. The electromagnetic loss is corrected according to the temperature of PMLSM to achieve the calculation convergence. After the velocity planning and temperature rise calculation, the maximum temperature of the PMLSM needs to be compared with the insulation limit temperature. The minimum requirement is the max temperature

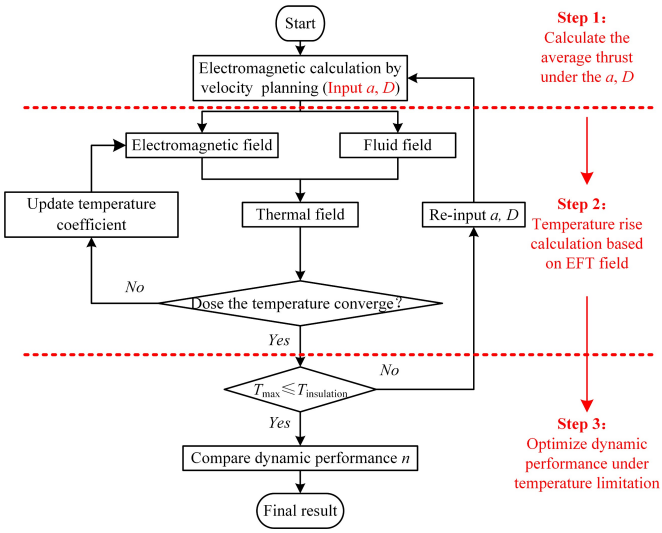

Fig. 11. Flowchart of the model of PMLSM at trapezoidal speed.

is lower than the insulation limit temperature. Otherwise, redo the velocity planning and re-input the acceleration a and the proportion of acceleration and deceleration time D. Finally, the most appropriate working conditions and dynamic performance will be selected by comparing the dynamic performance n under all reasonable velocity curves.

B. Temperature Rise Calculation

The acceleration a and the proportion of acceleration and deceleration time D of the CPMLSM are 15 m/s^2 and 76.9 % respectively under the rated working condition shown in Fig. 9 (c). The initial equivalent copper loss in one cycle is 32.10 W, whereas the final value is 39.82 W considering the effect of temperature. The difference between them is 7.72 W, which accounts for 19.39% of the initial equivalent copper loss. So it is particularly significant to consider thermal behavior of copper for PMLSM whose consumption is dominated by copper loss. What's more, the heat transfer coefficient of the air gap surface considering the acceleration and deceleration state is 36.40 W/(m^2·K) as shown in Fig. 10. The initial ambient temperature is 22 ℃.

Fig. 12 shows the temperature rises of different components of the CPMLSM under the rated working condition. The temperature rise of the windings is the highest and fastest because the windings are the main heat source and have high thermal conductivity and low specific heat capacity. The temperature of the epoxy resin adjacent to the windings is a little lower than that of the windings. Since the secondary contacts with the primary indirectly through the air, there is a great temperature difference between them. The average temperature of the primary is 82.78 ℃ and that of the secondary is 37.48 ℃. The temperature of the PMs is nearly the same as that of the back yoke.

The steady-state temperature distribution is shown in Fig. 13. The temperature of the primary gradually decreases from the center to both sides due to the poor conduction of insulating paint and epoxy resin. The maximum temperature of the primary reaches to 94.80 ℃ and the minimum temperature is 60.42 ℃. The overall temperature difference of the secondary is small due to the good thermal conductivity of the back yoke

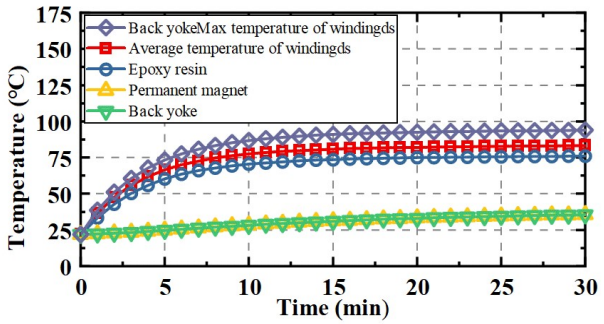

Fig. 12. Temperature rise curves of each component of CPMLSM under the rated working condition.

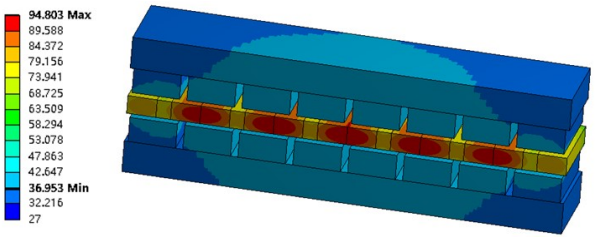

Fig. 13. Temperature distribution of CPMLSM in steady state under the rated working condition.

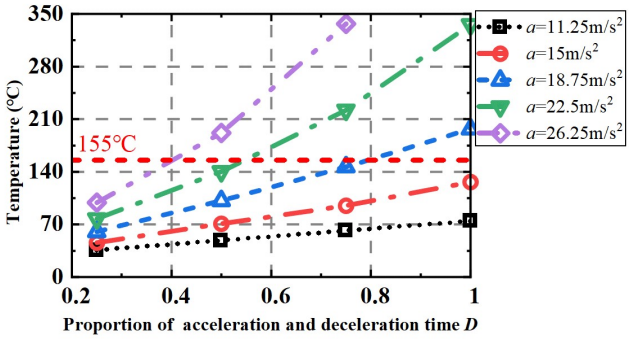

Fig. 14. Max temperature under different acceleration a, and proportion of acceleration and deceleration time D.

and PMs.

According to the analysis in Section III, the proportion of acceleration and deceleration time D and the acceleration a significantly influence heat source and boundary conditions of the thermal field, which are directly related to the temperature rise of PMLSM and its performance. Therefore, the maximum temperature of the CPMLSM under different proportion of acceleration and deceleration time D and acceleration a is calculated, as shown in Fig. 14.

From Fig. 14, when the proportion of acceleration and deceleration time D or acceleration a increases, the maximum temperature increases accordingly. The reason is that the acceleration a determines the winding currents, and the proportion of acceleration and deceleration time D determines the average loss. They directly affect the heat source density. In addition, for PMLSM with natural cooling, it is difficult to lower the temperature by increasing the mover speed through rising the proportion of acceleration and deceleration time D, which is consistent with the analysis in the previous section. Meanwhile, for this CPMLSM, the insulation grade is F and the maximum temperature it can withstand is 155 ℃. In this case, the selection of the proportion of acceleration and deceleration time D and deceleration a is limited in Fig. 14.

C. Motion Planning

For PMLSM with a certain stroke S, the number of round trips per second is determined by the acceleration a and the proportion of acceleration and deceleration time D concluded from (11). However, the dynamic performance n is determined by the proportion of acceleration and deceleration time D and improves with its increase when the acceleration a is constant. In this case, the average thrust remains unchanged. Therefore, the optimal dynamic performance at a fixed acceleration is determined by the maximum proportion of acceleration and deceleration time D_{max}. Combined with Fig. 14, the optimal dynamic performance of CPMLSM under different working conditions is shown in Table III.

TABLE III
OPTIMAL DYNAMIC PERFORMANCE UNDER DIFFERENT WORKING CONDITIONS

a (m/s^2)	D_{max}	Average thrust (N)	Dynamic performance n	Efficiency improvement
7.5	1	40	1.39	-27.60%
11.25	1	60	1.71	-10.94%
15	1	80	1.97	2.60%
15.94	1	85	2.03	5.73%
17.25	0.86	92	2.09	8.85%
18.75	**0.75**	**100**	**2.13**	**10.94%**
22.5	0.5	120	2.09	8.85%
26.25	0.37	140	2.03	5.73%
Rated working condition				
15	0.769	80	1.92	0

The maximum proportion of acceleration and deceleration time D_{max} firstly remains unchanged and then decreases slowly with the increase of acceleration a. This is because the thrust of the CPMLSM improves with the increase of the acceleration a, resulting in current rising. The proportion of acceleration and deceleration time D can only be adjusted to achieve a dynamic balance between the heat source density and the heat transfer coefficients. With the following, the dynamic performance and efficiency improvement changes. Fig. 15 shows the trend of the dynamic performance more intuitively based on Table III. The dynamic performance n at low thrust is superior to that at large thrust under some circumstances. There is an optimal value of dynamic performance. Moreover, when the acceleration a is 18.75 m/s^2 and the proportion of acceleration and deceleration time D is 75 %, the average thrust is 100 N and the dynamic performance n is improved from 1.92 to 2.13 times per second. The working efficiency is improved by 10.94 %.

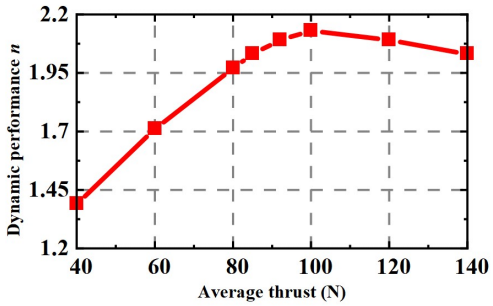

Fig. 15. Dynamic performance varies with average thrust.

V. EXPERIMENT VALIDATION

To verify the loss model considering the acceleration a and the proportion of acceleration and deceleration time D as well as the velocity planning model based on EFT field, an 8-pole/6-slot CPMLSM is manufactured and tested. Its structure parameters are consistent with Table I. Fig. 16 shows the test platform, which is mainly composed of the 8-pole/6-slot double-sided CPMLSM, drive controller, DC power supply, multimeter, etc.

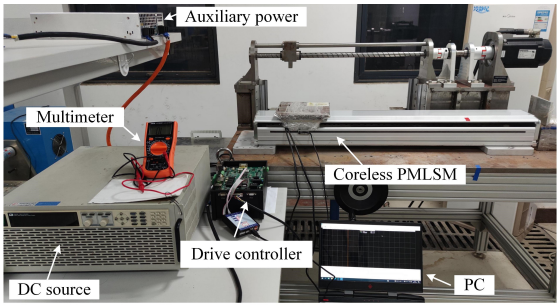

Fig. 16. Temperature measurement experiment platform.

When the CPMLSM makes periodic reciprocating motion, the heat transferring from the winding part to the secondary is limited. As a result, the temperature of the secondary is much smaller than that of the primary, which is consistent with the analysis in Section IV. Consequently, only the temperature rise of the windings is measured during the experiment, which is obtained by the electric resistance method.

$$\theta = \frac{R - R_i}{\alpha R_i} + \theta_i \tag{12}$$

where θ_i is the initial temperature; R_i is the initial winding resistance; R is the resistance when the winding temperature is θ; α is the resistance coefficient of the copper.

The primary windings are powered on with current density of 17 A/mm^2. The period T is 4 seconds. The percentage of power-on time account for 40 %, 60 % and 80 %, respectively. The initial ambient temperature is 22 ℃. By measuring the current and voltage during the temperature rise test, the resistance value is obtained. Then, the windings' temperature rise curves under the mover static state are obtained through formula (12), as shown in Fig. 17.

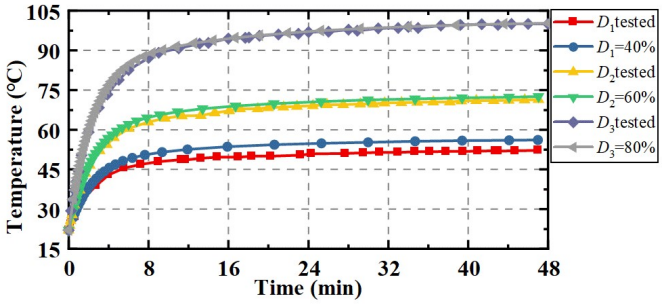

Fig. 17. Tested and calculated temperature rise curves of the windings with the current density of 17 A/mm^2 when the mover is static.

For the same current density (acceleration), the higher the proportion of power-on time (acceleration and deceleration time), the faster the temperature rises. In addition, even if the percentages of power-on time are different, the calculated temperature rise matches well with the tested one. When the

winding is up to about 48 minutes, the CPMLSM temperature rise reaches the steady state. Table IV shows the temperature of the windings in steady state. The temperature rise difference between simulation and test is within 5 ℃. What's more, with the increase of the proportion of power-on time, the temperature rise difference gradually decreases.

TABLE IV
TESTED AND CALCULATED
WINDING TEMPERATURES IN STEADY STATE

D	Simulation (℃)	Experiment (℃)	Difference (℃)
40%	52.14	56.16	4.02
60%	72.5	71.37	1.13
80%	100.3	100	0.3

Meanwhile, the CPMLSM is controlled by the drive controller and the thermal behavior is investigated by the dynamic experiment. Fig. 18 shows the measured three-phase currents and mover velocity when the proportion of acceleration and deceleration time D accounts for 25 %. It is necessary to supply current to overcome the friction when the mover is at uniform speed. The current difference between the acceleration and deceleration is small due to the poor frictional force. Moreover, the current during acceleration and deceleration is much larger than that at uniform speed as analyzed in Section III. The whole current curves change periodically. The tested velocity can well follow the target one, which means the dynamic performance of the CPMLSM can reach the design requirements.

Fig. 19 compares the tested and calculated temperature rise under four working conditions. The stroke S is 0.3 m. When the acceleration a is 8 m/s^2, the proportion of acceleration and deceleration time D is 25%, 50% and 75%, respectively. In addition, the working condition of a= 5 m/s^2 and D= 75 % is taken as a contrast to that of a = 8 m/s^2 and D = 75%. The winding energization duration under the above working conditions is 600, 420, 240 and 240 seconds, respectively. The initial ambient temperature is 18 ℃. The maximum temperature error between the test and calculation is within 5.5 ℃, while that not considering acceleration and deceleration reaches 10 ℃. This illustrates that the thermal model considering the acceleration and deceleration greatly improves the calculation accuracy.

In addition, the winding temperature grows significantly as the acceleration a or the proportion of acceleration and deceleration time D rises although the dynamic performance improves. Hence, either of them needs to be reduced to limit the temperature rise. The dynamic performance n is 1.25 times under the working condition of a = 8 m/s^2 and D = 75%, whereas the same is 0.992 times under the working condition of a = 5 m/s^2 and D = 75%. However, the temperature drops by 80 ℃, which leaves a large margin for velocity planning and dynamic performance optimization, where the balance between the acceleration a and the proportion of acceleration and deceleration time D is crucial. What's more, the dynamic performance n is 0.865 times under the working condition of a = 5 m/s^2 and D = 75 % while the same is 0.992 times under the working condition of a = 8 m/s^2, D = 25 %, which means the

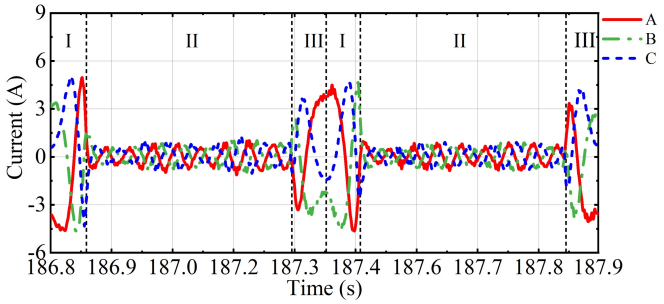

I：Acceleration. II：Uniform speed. III：Deceleration.

(a)

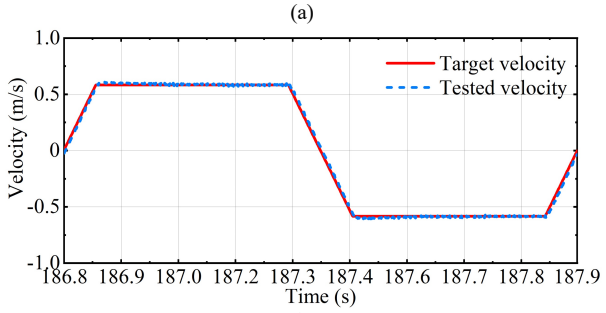

(b)

Fig. 18. (a) Measured three-phase currents. (b) Velocity curves.

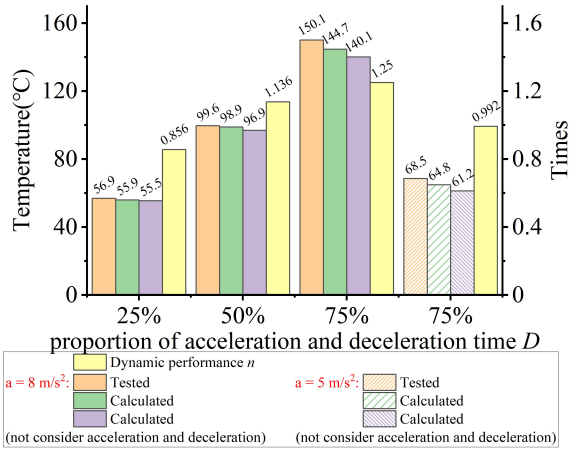

Fig. 19. Tested and calculated temperature rise under four working conditions.

low thrust can be selected and the requirement for power supply is reduced. In a word, it demonstrates the correctness of the velocity planning model of PMLSM at trapezoidal speed based on EFT field. On the other hand, the model presented here is a quite efficient tool for the thermal behavior and dynamic performance assessment of the PMLSM.

VI. CONCLUSION

Aiming at the working condition of frequent acceleration and deceleration of PMLSM, a velocity planning model based on EFT field, considering the proportion of acceleration and deceleration timed D and the acceleration a, is proposed to improve the temperature rise calculation accuracy and optimize the dynamic performance. Through simulation calculation and experimental verification, the following conclusions can be obtained:

1) The winding loss model based on acceleration a and the proportion of acceleration and deceleration time D can predict the temperature rise accurately. The temperature rise

experiment of an annular winding sample shows that the error by this loss model is not more than 5 %.

2) The acceleration and deceleration of the PMLSM significantly affect the fluid state and velocity in the air gap, which is the key to calculate the convective heat dissipation coefficient. Due to the acceleration and deceleration, the air velocity in the air gap is significantly lower than that considering the only uniform motion.

3) Through the velocity planning model based on EFT field, the optimal dynamic performance of the motor under the insulation limit is obtained. Through the simulation calculation and experiment of an 8-pole/6-slot coreless PMLSM, the dynamic performance n increases from 1.92 to 2.13, by 10.94%.

In addition, the temperature rise calculation model and velocity planning method in this paper can be used not only for trapezoidal speed modes, but also for triangular, sinusoidal and other speed or position response conditions. In application, the loss calculation and heat transfer coefficient should be revised according to the specific situation.

REFERENCES

[1] H. S. Lim, R. Krishnan, and N. S. Lobo, "Design and Control of a Linear Propulsion System for an Elevator Using Linear Switched Reluctance Motor Drives," *IEEE Trans. Ind. Electron.*, vol. 55, no. 2, pp. 534–542, 2008.

[2] J. Y. Yoon, J. H. Lang, and D. L. Trumper, "Double-Sided Linear Iron-Core Fine-Tooth Motor for Low Acoustic Noise and High Acceleration," *IEEE/ASME Trans. Mechatron.*, vol. 24, no. 5, pp. 2161–2170, Oct. 2019.

[3] S.Y. Jung, S.Y. Kwak, S.K. Hong, C.G. Lee, and H.K. Jung, "Design consideration of steel-cored PMLSM for short reciprocating travel displacements," in *Proc. of IEEE International Electric Machines and Drives Conference*, IEMDC'03., Madison, WI, USA, 2003, vol. 2, pp. 1061–1067.

[4] G. Dudgeon, I. Braverman, and K. Tamminana, "Modeling and Simulation in Support of System Level Design for High Acceleration Linear Motors," *Proc. IEEE*, vol. 97, no. 11, pp. 1818–1830, Nov. 2009.

[5] H. Ding and J.H Wu, "Point-to-Point Motion Control for a High-Acceleration Positioning Table via Cascaded Learning Schemes," *IEEE Trans. Ind. Electron*., vol. 54, no. 5, pp. 2735–2744, Oct. 2007.

[6] Y. Hasegawa and Y. Aoyama, "Development of high-acceleration linear motor system using the transient loss evaluation," in *Proc. of 2017 11th International Symposium on Linear Drives for Industry Applications (LDIA)*, Osaka, Sep. 2017, pp. 1–6.

[7] L. Yan, Z. Dong, and S. Zhang, "Thermal Analysis of a Novel Linear Oscillating Machine Based on Direct Oil-Cooling Windings," *IEEE Trans. Energy Convers*., pp. 1–1, 2021.

[8] W. Tong, R. Sun, S. Li, and R. Tang, "Loss and Thermal Analysis for High-Speed Amorphous Metal PMSMs Using 3-D Electromagnetic-thermal Bi-Directional Coupling," *IEEE Trans. Energy Convers*., vol. 36, no. 4, pp. 2839–2849, Dec. 2021.

[9] X. Sun, B. Wan, G. Lei, X. Tian, Y. Guo, and J. Zhu, "Multiobjective and Multiphysics Design Optimization of a Switched Reluctance Motor for Electric Vehicle Applications," *IEEE Trans. Energy Convers.*, vol. 36, no. 4, pp. 3294–3304, Dec. 2021.

[10] W. Geng, T. Zhu, Q. Li, and Z. Zhang, "Windings Indirect Liquid Cooling Method for a Compact Outer-Rotor PM Starter/Generator With Concentrated Windings," *IEEE Trans. Energy Convers.*, vol. 36, no. 4, pp. 3282–3293, Dec. 2021.

[11] K. Li, S. Wang, and J. P. Sullivan, "A novel thermal network for the maximum temperature-rise of hollow cylinder," *Applied Thermal Engineering,* vol. 52, no. 1, pp. 198–208, Apr. 2013.

[12] X. Huang, L. Li, B. Zhou, C. Zhang, and Z. Zhang, "Temperature Calculation for Tubular Linear Motor by the Combination of Thermal Circuit and Temperature Field Method Considering the Linear Motion of Air Gap," *IEEE Trans. Ind. Electron*., vol. 61, no. 8, pp. 3923–3931, Aug. 2014.

[13] X. Liu, H. Yu, Z. Shi, T. Xia, and M. Hu, "Electromagnetic-fluid-thermal field calculation and analysis of a permanent magnet linear motor," *Applied Thermal Engineering*, vol. 129, pp. 802–811, Jan. 2018.

[14] Y. Chen, Q.F. Lu, Y.M. Shen, "Electromagnetic-thermal coupled analysis of water-cooled double-sided permanent magnet linear synchronous machines," *Proc. CSEE*. vol. 39, no. 7, pp. 1852-1861.

[15] L. Li, X. Huang, and B. Kou, "Air flow of the linear motor for electromagnetic launch system," in *Proc. of 2012 16th International Symposium on Electromagnetic Launch Technology*, Beijing, China, May 2012, pp. 1–5.

[16] D.N. Kim, I.M. Chen, and T.C. Ng, "Planning algorithms for s-curve trajectories," in *Proc. of 2007 IEEE/ASME international conference on advanced intelligent mechatronics*, Zurich, Switzerland, 2007, pp. 1–6.

[17] J. Ning, J. Xia, C. Wang, and B. Peng, "Optimal and planning of motion for reducing vibration on PMLSM linear drive system of high-precision high -speed CNC machine tool," in *Proc. of 2011 International Conference on Transportation, Mechanical, and Electrical Engineering (TMEE)*, ChangChun, China, Dec. 2011, pp. 580–583.

[18] M. Yuan, Z. Chen, B. Yao, and X. Liu, "Fast and Accurate Motion Tracking of a Linear Motor System Under Kinematic and Dynamic Constraints: An Integrated Planning and Control Approach," *IEEE Trans. Contr. Syst. Technol*., vol. 29, no. 2, pp. 804–811, Mar. 2021.

[19] Z. Pei, J. Zhao, J. Song, K. Zong, Z. He, and Y. Zhou, "Temperature Field Calculation and Water-Cooling Structure Design of Coreless Permanent Magnet Synchronous Linear Motor," *IEEE Trans. Ind. Electron*., vol. 68, no. 2, pp. 1065–1076, Feb. 2021.

[20] Q. Lu, X. Zhang, Y. Chen, X. Huang, Y. Ye, and Z. Q. Zhu, "Modeling and Investigation of Thermal Characteristics of a Water-Cooled Permanent-Magnet Linear Motor," *IEEE Trans. on Ind. Appl*., vol. 51, no. 3, pp. 2086–2096, May 2015.

[21] L. Zhang et al., "Comparison Between Dual-Armature Linear Switched Flux Permanent Magnet Machine and Linear Surface-Mounted Permanent Magnet Machine Considering Thermal Conditions," *IEEE Trans. Energy Convers*., vol. 36, no. 4, pp. 3522–3532, Dec. 2021.

[22] S. Cui, W. Zhao, and S. Wu, "Research on the Thermal Field and Active Water Cooling System Design of an Air-Core Compulsator," *IEEE Trans. Plasma Sci.*, vol. 39, no. 1, pp. 257–262, Jan. 2011.

[23] Y. Tang, L. Chen, F. Chai, and T. Chen, "Thermal Modeling and Analysis of Active and End Windings of Enclosed Permanent-Magnet Synchronous In-Wheel Motor Based on Multi-Block Method," *IEEE Trans. Energy Convers*., vol. 35, no. 1, pp. 85–94, Mar. 2020.

[24] A. Rasekh, P. Sergeant, and J. Vierendeels, "Convective heat transfer prediction in disk-type electrical machines," *Applied Thermal Engineering*, vol. 91, pp. 778–790, Dec. 2015.

[25] Z. Zhao, Thermal Transmission. Beijing, China: Higher Education Press, 2002.

[26] S. Yang, W. Tao write, Heat Transfer, fourth ed., Higher Education Press, China, 2006.

Xuzhen Huang (M'14) received the B.E., M.E., and Ph.D. degrees in electrical engineering from the Harbin Institute of Technology, Harbin, China, in 2006, 2008, and 2012, respectively. She is with the Jiangsu Key Laboratory of New Energy Generation and Power Conversion, Nanjing University of Aeronautics and Astronautics, Nanjing, China, where she is currently a Professor of Electrical Engineering. Her current research interests include the linear permanent magnet synchronous motors and the thermal analysis of motors.

Zheng Wang received the B.E. degree in electrical engineering in 2020, from the Nanjing University of Information Science and Technology, Nanjing, China. Now, he has been working toward the M.S. degree in electrical engineering in the Nanjing University of Aeronautics and Astronautics, Nanjing, China. His current research interests include the electrical machines and multiphysics analysis of linear motor.

Yiwei Zhang received the B.S. degree in electrical engineering from Nanjing University of Aeronautics and Astronautics, Nanjing, China, in 2020. He is currently working toward the Ph.D. degree in electrical engineering at Nanjing University of Aeronautics and Astronautics, Nanjing, China. His research interests include system identification and motor drive with application in high-precision mechanical servo systems.

Qiang Tan, was born in Jiang Su, China, in 1991. He received the B. E. and M. E degrees in electrical engineering from Nanjing University of Aeronautics and Astronautics, Nanjing, China, in 2014 and 2017, respectively. He received the D. E degree in electrical engineering from Harbin Institute of Technology, Harbin, China., in 2021. He is working in the Automation College, Nanjing University of Aeronautics and Astronautics, where he is currently an associate professor. His current research focus on the linear permanent magnet synchronous motors.